ORIGINAL PAPER

Fluorescence Imaging of Heat-Stress Induced Mitochondrial Long-Term Depolarization in Breast Cancer Cells

**Cathrin Dressler · Juergen Beuthan ·
Gerhard Mueller · Urszula Zabarylo · Olaf Minet**

Abstract Various thermotherapies are based on the induction of lethal heat in target tissues. Spatial and temporal instabilities of elevated temperatures induced in therapy targets require optimized treatment protocols and reliable temperature control methods during thermotherapies. Heat-stress induced effects on mitochondrial transmembrane potentials were analyzed in breast cancer cells, species MX1, using the potential sensor JC-1 (Molecular Probes, Invitrogen, Germany). Potential dependant labeling of heat-stressed cells was imaged and evaluated by fluorescence microscopy and compared with control cells. JC-1 stains mitochondria in cells with high mitochondrial potentials by forming orange-red fluorescent J-aggregates while in cells with depolarized or damaged mitochondria the sensor dye exists as green fluorescent monomers. In MX1 cells orange-red and green fluorescence intensities were correlated with each other after various heat-stress treatments and states of mitochondrial membrane potentials were deduced from the image data. With increasing stress temperatures the intensity of red fluorescent J-aggregates decreased while the green fluorescence intensity of JC-1 monomers increased. This heat-stress response happened in a nonlinear manner with increasing temperatures resulting in a nonlinear increase of red/green fluorescence ratios. These data indicated that mitochondria in MX1 cells were increasingly depolarized in response to increasing ambient temperatures.

Introduction

Heat represents a primarily environmental stress factor inducing multiform stress reactions in cells and tissues exposed to unphysiologically elevated temperatures. Molecular mechanisms triggered by heat stress include enhanced synthesis of so-called heat shock proteins (HSP) providing a limited protection of cells and organisms against heat-induced damages [1–4]. HSP are also involved in other stress responses initiated by non-thermal stress factors, like oxidative stress, energy and nutrient depletions, or drug toxicities [4]. The effectiveness of HSP mediated damage protections depend on the stress factor dose, exposure time, and the cell species encountering stress. Especially heat stress induces cell type individual stress reactions [2]. Detailed knowledge about molecular HSP functions and the resulting metabolic interactions does not exist so far [4].

In the field of clinical cancer therapy two major groups comprise thermotherapy: 1. laser-induced thermotherapy inducing local temperatures between $60°C$ and $100°C$ [5–7] and 2. hyperthermia working with temperatures below $45°C$ [8]. Combined modality treatments such as hyperthermia-assisted radiotherapy and/or chemotherapy are under intensive investigation today [8–11]. A further thermotherapeutic approach has been published by Jordan et al. (2001) and Johannsen et al. (2005) who suggested injection of magnetic nanoparticles into a tumor followed by application of

C. Dressler (✉)
Laser- und Medizin-Technologie GmbH,
Fabeckstrasse 60-62,
D-14195 Berlin, Germany
e-mail: c.dressler@lmtb.de

J. Beuthan · G. Mueller · U. Zabarylo · O. Minet
Institut fuer Medizinische Physik und Lasermedizin, Charité
Campus Benjamin Franklin, Universitaetsmedizin Berlin,
Berlin, Germany

alternating current magnetic fields inducing elevated temperatures in the nanoparticle-loaded tissue [12, 13]. Generally, if the temperature induced in a target tissue is high enough to cause lethal effects and to induce thermal destruction thermotherapy is successful [5–11]. Since heat transfer and distribution in a target usually are irregular and exhibit spatial and temporal instabilities there is always a risk that areas of the thermotherapeutic target survive the intervention and cause persistence or recurrence of disease [7, 14, 15]. Thresholds for thermal damage in human tissues vary among tissue species as well as among normal and diseased tissues [16, 17]. Several reports have demonstrated mitochondria to be major targets of heat stress inside eukaryotic cells [18–22].

Fluorescent probes for the measurement of membrane potential have been under steady development since the pioneering work of Waggoner [23]. In the present study we investigated the heat responsibilities of mitochondria in MX1 breast carcinoma cells by membrane potential-dependant fluorescence labeling. The mitochondrial transmembrane potential sensor JC-1 (Molecular Probes, Invitrogen, Germany) was used. In intact and highly polarized mitochondria JC-1 accumulates as orange-red fluorescent J-aggregates while in damaged cells with depolarized mitochondrial membranes the dye forms green fluorescent monomers. Therefore the relation between red and green fluorescence intensities describes mitochondrial transmembrane potentials ($\Delta\Psi_m$) and gives evidence of the physiological or pathological state of the cells under investigation [24]. Spectral properties of monomeric and multimeric forms of the JC-1 sensor dye are illustrated in Fig. 1.

Depending on the stress temperature cells were exposed to, the mitochondria were more or less depolarized leading to an increase in green fluorescent JC-1 monomers accompanied by a decrease in orange-red J-aggregates. This effect was rather weak under comparatively mild heat stress conditions between 40°C and 45°C while under severe stress at 50°C or 56°C the response was more pronounced and clearly documented by very low $\Delta\Psi_m$. Mitochondria in MX1 cells consequently react to heat stress in depolarizing

of transmembrane potentials with temperature-dependant extents.

Experimental

Cell cultivation

Human undifferentiated breast cancer cells of the species MX1 (Deutsches Krebsforschungszentrum, Germany) were employed as tissue model. Cells were maintained in RPMI 1640 medium supplemented with 20 mM HEPES buffer, 10% (v/v) heat inactivated fetal calf serum, 1% antibiotic-antimycotic solution (100 U/mL penicillin, 100 μg/mL streptomycin, 0.25 μg/mL amphotericin B (PAA Laboratories GmbH, Germany) at 37°C. Monolayer cultures were dissociated with 0.05% trypsin-0.02% EDTA (PAA Laboratories GmbH, Germany). All other culture medium components and solutions were purchased from Biochrom KG seromed, Germany. Experimental cells were grown in glass chamber slides (Nunc GmbH & Co. KG, Germany) until subconfluent cell densities were achieved.

Heat stressing

Heat-stress treatments were performed in a temperature-regulated water bath at the temperatures given with the results (40°C, 42°C, 45°C, 50°C, or 56°C) for 30 min each. Control cells were not submitted to heat stress but were continuously kept at 37°C. Immediately after heat stressing cells were submitted to subsequent experimental processing.

Mitochondrial fluorescence labeling

The mitochondrial membrane potential sensor JC-1 (5,5′, 6,6′-Tetrachloro-1,1′,3,3′-tetraethyl-imidacarbocyanine iodide; Molecular Probes, Invitrogen, Germany) was used to label mitochondria in transmembrane potential dependant manner. The JC-1 stock solution was prepared in anhydrous

Fig. 1 Absorption and fluorescence spectra of JC-1 monomer and J-aggregate [25]
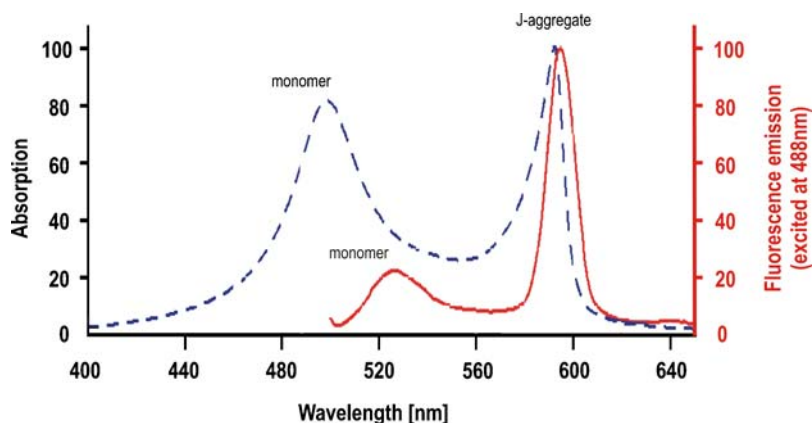
dimethyl sulphoxide and diluted in supplemented culture medium with an end concentration of $9.4\,\mu$molar. In physiologically polarized cells JC-1 accumulates at mitochondria as red fluorescent J-aggregates while in depolarized cells the dye forms green fluorescent monomers. Spectral properties of JC-1 are illustrated in Fig. 1 [25]. The labeling procedure was applied following the heat treatments according to the manufacturer's recommendations [26].

Fluorescence microscopy

Mitochondrial fluorescences were imaged with a wide-field epifluorescence microscope Axiovert 200 M (Carl Zeiss, Germany) combined with a digital color camera AxioCam MRc (Carl Zeiss, Germany). JC-1-labeled cells were imaged with the red fluorescence channel ($\lambda_{excitation}$: 546 ± 12 nm band pass filter, $\lambda_{detection}$: >590 nm long pass filter) and the green fluorescence channel ($\lambda_{excitation}$: 450–490 nm band pass filter, $\lambda_{detection}$: >515 nm long pass filter) each. Illumination times required for optimal fluorescence image acquisition were digitally measured by the AxioCam MRc camera for every image with a variation range from 268 to 2354 ms.

Statistical evaluation

Ratios of the fluorescence amplitudes measured in the red and the green channel were evaluated for every image frame after correcting the amplitudes with the illumination times applied in each case. The average value in every temperature group was used for statistical assessments of red and green fluorescence intensities.

Results

MX1 cells were labeled with the mitochondrial membrane potential sensing marker JC-1 in order to monitor heat-stress induced effects on $\Delta\Psi_m$. The fluorescence micrographs in Fig. 2 clearly show membrane potential correlated labeling of mitochondria in MX1 cells. With increasing stress temperatures at 40°C, 42°C, 45°C, 50°C, or 56°C the $\Delta\Psi_m$ dependant orange-red and green fluorescence intensities in MX1 cells labeled with JC-1 were altered when compared with control cells. The orange-red fluorescence of J-aggregates at mitochondria with high $\Delta\Psi_m$ was imaged in both fluorescence channels while green fluorescence of monomeric JC-1 of course was only imaged in the green channel.

After the mitochondria in the control group and in the 40°C, 42°C, and 45°C stress groups exhibited orange-red fluorescence the signal color in the red channel was changed in the 50°C and 56°C stress groups. Stress temperatures at
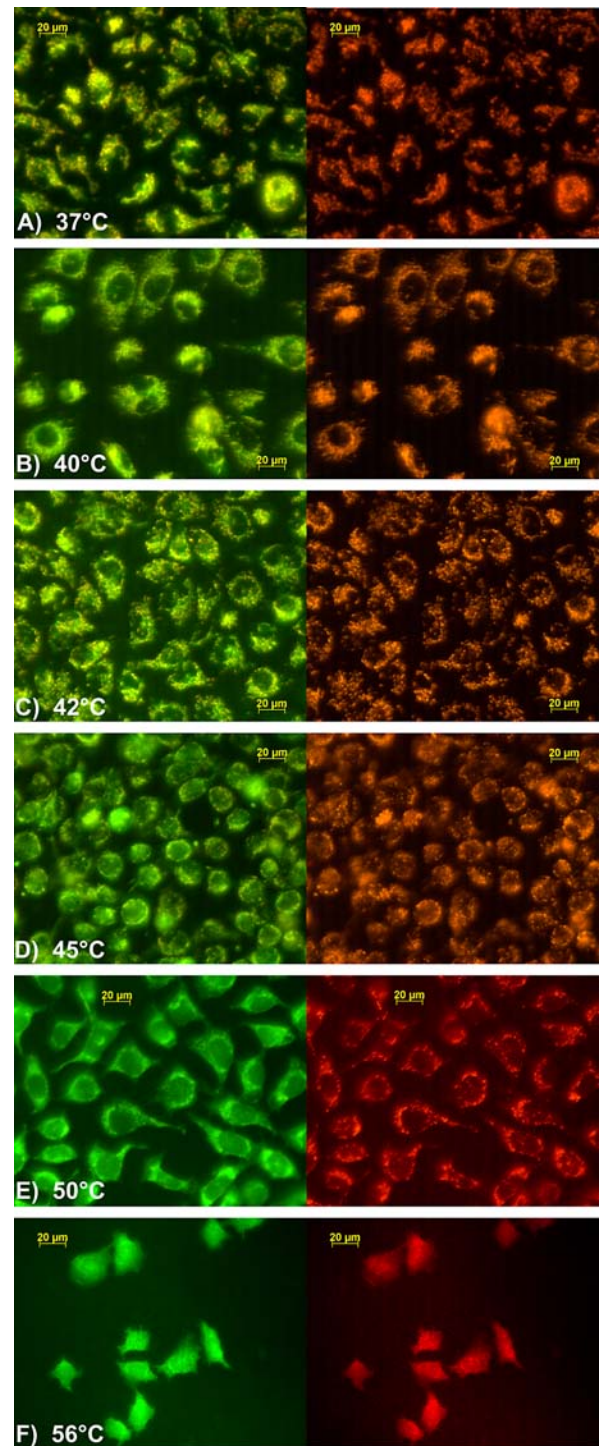

Fig. 2 Green (*left*) and red (*right*) fluorescence of heat-stressed MX1 cells after mitochondrial transmembrane potential dependant labeling with JC-1 (Molecular Probes, Invitrogen Germany). Panel A shows control cells incubated at 37°C, panels B-F show heat-stressed cells treated with the temperatures indicated at every panel for 30 min, each. Illumination times employed for acquiring the images were: (panel A) 645 ms green, 268 ms red; (panel B) 580 ms green, 295 ms red; (panel C) 711 ms green, 633 ms red; (panel D) 571 ms green, 656 ms red; (panel E) 765 ms green, 1172 ms red; (panel F) 677 ms green, 2345 ms red

Fig. 3 Average ratios of fluorescence amplitudes measured in the red and the green fluorescence channel. Red/green ratios are indicating changes of the quantitative relation between orange-red fluorescent J-aggregates in MX1 cells with high $\Delta\Psi_m$ and green fluorescent JC1 monomers in cells with low $\Delta\Psi_m$. Standard deviations are given as mean square deviations
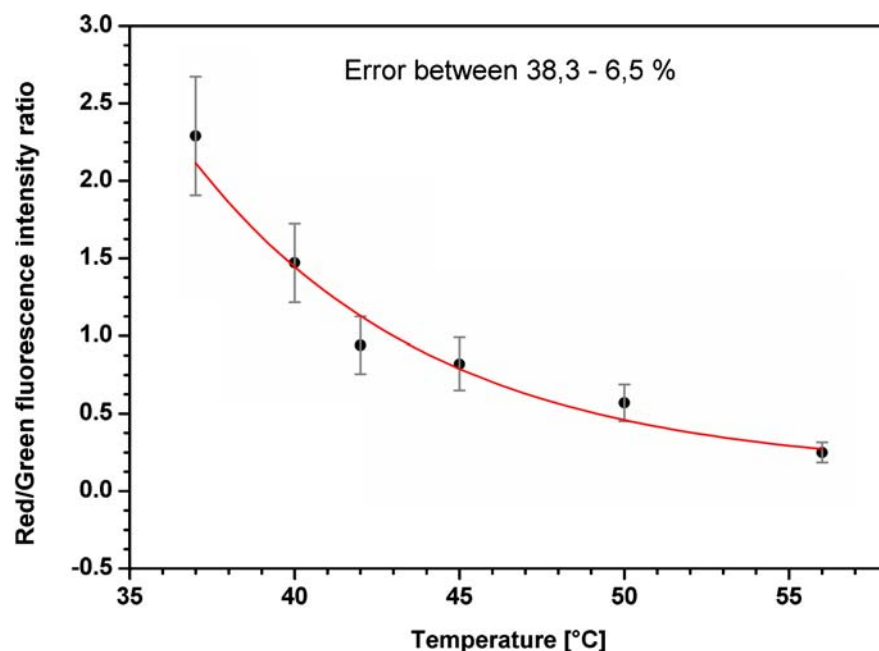
50°C or 56°C caused JC-1 to show deep red fluorescence (Fig. 2).

A direct readout of fluorescence intensities imaged in both channels for every object was not possible since acquisition times used for making the images were digitally adjusted with the purpose of optimal fluorescence imaging. Therefore the ratio of fluorescence amplitudes measured in the red and the green channel was evaluated (red/green ratio) for every object or every image pair, respectively. Average red/green ratios of the control group and the different heat-stress groups were plotted against the temperatures cells were treated with (Fig. 3). The red/green fluorescence ratios turned out to decrease with increasing stress temperatures in a nonlinear manner, because orange-red fluorescence intensities discontinuously decreased while green fluorescence intensities increased and consequently the red/green ratios declined.

The nonlinear interrelation between mitochondrial depolarization and stress temperature is presented by the exponential function shown in Fig. 3. Whereas the red-to-green fluorescence intensity ratios decayed rather rapidly in the temperature range between 40°C and 45°C switching over to a decelerated decay at higher temperatures following an exponential curve progression

Generally these results indicated that the amount of red fluorescent J-aggregates accumulating at mitochondria with comparatively high membrane potentials decreased with increasing stress temperatures opposite to the enhanced green fluorescence of J-monomers in cells with more or less depolarized $\Delta\Psi_m$. In the control group the red/green ratio was approximately 1.7. Under mild heat stress conditions at 40°C or 42°C the red/green ratios only slightly decreased compared with control cells. The ratios in these groups were

approximately 1 or above 1 denoting that orange-red signal intensities of J-aggregates fluorescence were higher than green fluorescence signal intensities. With higher stress temperatures at 45°C and 50°C ratios drastically decreased with values below 0.7, because as expected red fluorescence intensities were weaker than green fluorescence intensities. Exposing cells to 56°C heat resulted in pan-cellular green and red fluorescence distributions whereas the green signal intensities were much higher than red signal intensities which only represented residual background fluorescence. Therefore in the 56°C stress group the average red/green ratio again was drastically decreased when compared with the 50°C stress group to reach a value of approximately 0.2 showing that red fluorescence intensity was approximately 20% of the green fluorescence intensity measured in this experimental group. The red signal intensity decrease resulted from massive depolarization of $\Delta\Psi_m$ under exposure to 56°C heat accompanied by structural organelles destruction enhancing green fluorescence of JC-1 monomers inside severely damaged MX1 cells.

The fluorescence intensity distributions inside cells imaged in the red and the green fluorescence channel were derived as three-dimensional (3D) illustrations. Characteristic examples of 3D fluorescence intensity profiles are shown in Fig. 4. Here the fluorescence amplitudes were corrected with the respective image acquisition times in order to compare distributions of absolute signal intensities with each other. Each 3D image is z scaled to the maximum of fluorescence intensity. The red fluorescence intensity maxima (RFIM) were highest and nearly constant in the temperature range between 37°C and 42°C. From a stress temperature of 45°C on RFIM drastically declined while the green
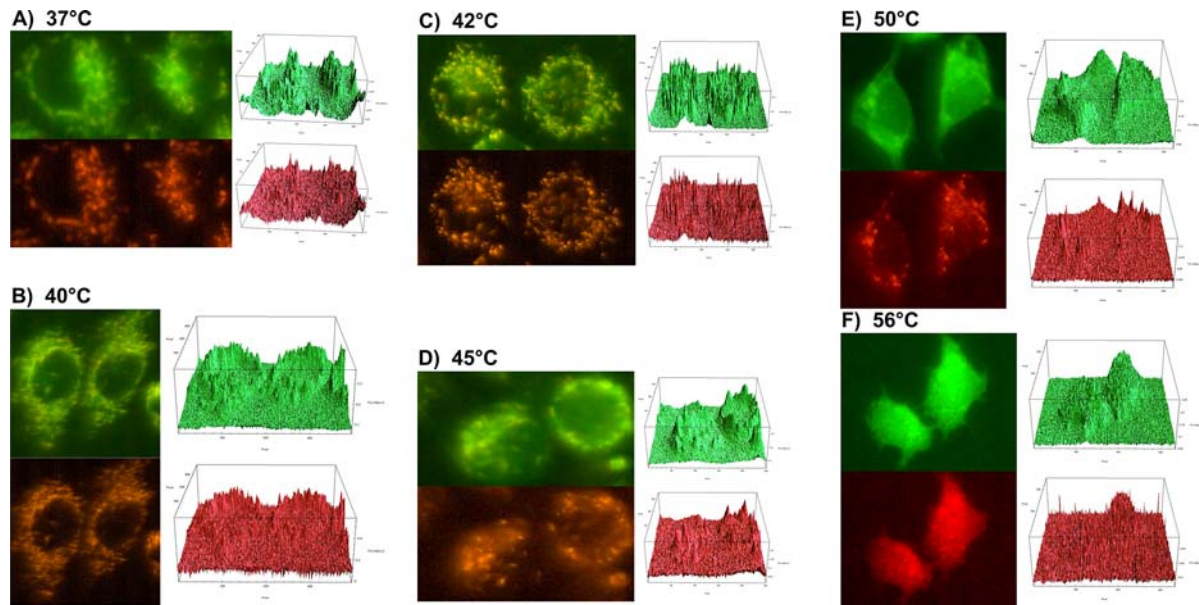
Fig. 4 Green and red fluorescence distributions in heat-stressed MX1 cells after mitochondrial membrane potential dependant labeling with JC-1 (Molecular Probes, Invitrogen Germany). The regions of interest (*left*) were divided into red (*bottom*) and green (*top*) data fraction for the green fluorescence channel (atop in every panel) and red fluorescence channel (at the bottom of every panel) each and illustrated as 3D fluorescence distributions. Panel A shows control cells incubated at 37°C, panels B-F show heat-stressed cells treated with the temperatures indicated at every panel for 30 min, each. Two cells are shown in every panel

fluorescence intensity maxima (GFIM) exceeded RFIM. This again indicated the increasing depolarization of mitochondria in response to heat stress.

Discussion

The aim of the present study was to investigate mitochondrial responses to heat stress in the temperature range between 40°C and 56°C (30 min each) in breast cancer cells species MX1. As stress-sensitive indicator the mitochondrial transmembrane potential ($\Delta\Psi_m$) was analyzed by fluorescence microscopy after mitochondria-selective staining with JC-1. Several studies have documented $\Delta\Psi_m$ to be a parameter sensitive to various kinds of environmental stress [24, 27–29]. Since heat also represents an environmental stress factor we were interested in the cellular $\Delta\Psi_m$ response to elevated temperatures.

Hyperthermia has been proposed as a potential therapeutic application in clinical cancer therapy [8]. The cellular mechanisms involved in heat-stress responses and their impact on various subcellular structures so far have only been described for selected model tissues. Funk et al. (1999) studied heat-stress induced changes of mitochondrial morphologies in astrocytes and MDCK cells by video-enhanced contrast microscopy using a perfusion cell chamber system [18]. In their study the morphological alterations inside mitochondria exposed to appropriate heat stress conditions were revealed to be reversible. Recovery of mitochondrial changes subse-

quent to heat treatment was also detected in microglial cells [21]. Metabolic investigations on microglial cells revealed dropping of the physiological ATP content by 60% 1 h after a 20 min heat shock at 45°C. This indicated that heat stress leads to scaling down of the energy resource ATP in this cell type [22]. In heat-shocked rats failing of energy metabolism and ATP depletion were detected as the earliest cell-damaging factors of ischemic insult [30].

Several subcellular structures were already analyzed in MX1 cells after heat stress. Here the F-actin cytoskeleton was detected to be thermally more sensitive than the plasma membrane since F-actin fibers exhibited morphological alterations under comparatively mild heat stress (40°C and 42°C) while plasma membranes were morphologically not altered by these heat-stress conditions [31]. Only temperatures higher than 42°C induced detectable morphological changes in plasma membranes [31, 32]. These results did not give any information about the functionalities of the investigated cell components. It was shown previously that MX1 cell viability was not attenuated after heat stress at 40°C or 42°C. When exposed to 45°C or higher temperatures cell viabilities were increasingly diminished. Comparing these results it should be concluded that reorganization of F-actin cytoskeletons resulted from an active stress response under heat stress at 40°C or 42°C which is supposed to be compensated during recovery of heat-stressed cells. It was also demonstrated earlier that MX1 cells undergo necrosis during 30 min treatment at 56°C but not at 50°C or lower stress temperatures, because cells exposed

to 50°C did not exhibit necrotic phenotypes [32]. Therefore complete depolarization of mitochondria in cells stressed at 56°C was a consequent result of necrosis. Mitochondrial permeability transition in general is an early sign of the initiation of cellular apoptosis or necrosis provoking a collapse in the electrochemical gradient across mitochondrial membranes [24, 33, 34].

Especially cellular responses to sublethal stress temperatures, as used for different therapeutic hyperthermia applications, are essential for the understanding of heat-induced effects in tissues. Mild or severe heat stress are not unequivocally definable and depend on cell species, tissue origin, cell cycle, developmental stages, as well as exposure times. Possibly there exists a rough borderline between lethal and sublethal heat stress [17].

As the central gateway of cellular energy metabolism mitochondria present cardinal targets of heat stress and other nonthermal stress factors [18–21]. Mitochondrial dysfunctions lead to an important decrease in cellular ATP levels and phosphorylation efficiencies [30].

Depolarization of mitochondria was detected in MX1 cells after heat stress whereas a nonlinear interrelation between mitochondrial depolarization dynamics and stress temperatures was revealed. This response was reflected by an exponential decay function describing the average ratios of fluorescence amplitudes measured for the membrane potential indicator JC-1 in the red and the green fluorescence channel (Fig. 3). The standard deviation, which is relatively large, can be reduced by increasing the number of investigated microscopical images.

It should be emphasized that only the red fluorescent J-aggregates measure the $\Delta\Psi_m$–dependant accumulation at mitochondria and the green fluorescence depends on passive binding of JC-1 monomers to any cellular membrane. Therefore it should be considered that the fluorescence intensity ratios of red and green emissions relate to phenomena occurring in different cellular regions. [35]. Since orangered fluorescence of aggregated JC-1 is strictly dependant on high $\Delta\Psi_m$ the fluorescence intensity ratios measured in this study do reflect the heat-stress induced depolarization of mitochondria.

The nonlinear response of MX1 mitochondria to heat stress corresponded well with our results obtained using various microscopic techniques for investigating heat-stress response of different subcellular structures in MX1 cells [31]. In our previous studies also nonlinear responses of metabolic activity, plasma membranes, and cytoskeletons in heat-stressed MX1 cells were observed [31, 32].

Applications of heat as therapeutic agent are affected by spatial and temporal variations of temperature distributions inside a target tissue and surrounding structures [16]. It is also possible that different subcellular components in a certain cell species may exhibit various heat sensitivities. Consequently thermal destruction inducing therapies generally demand for highly thorough as well as individual intervention protocols concerning the volume and location of diseased tissue, blood supply, application and control techniques, and the patient's physical condition.

Conclusions

Our investigations on mitochondrial depolarization in JC-1-labeled MX1 breast cancer cells revealed minor reductions of mitochondrial transmembrane potentials after heat stress in a temperature range between 40°C and 45°C compared with control cells. When more severe heat-stress conditions were applied at 50°C or 56°C mitochondria were completely depolarized shown by the intensive decrease in orange fluorescence intensities shifting to weak red fluorescence. Orange fluorescence was emitted by J-aggregates accumulated at mitochondria with comparatively high transmembrane potentials. In cells containing depolarized mitochondria JC-1 formed green fluorescent monomers. Heat-induced depolarization of mitochondria was monitored by the average ratios evaluated for the fluorescence amplitudes measured for mitochondrial membrane potentials (red:green ratios). The red:green ratios measured in the red and the green fluorescence channel for every stress temperature tested in this study is reflected by an exponential decay function (Fig. 3). This finding is different from the spontaneous depolarization as observed in myocytes after application of FCCP (4-(trifluoromethoxy) phenylhydrazone) [36].

References

1. Lindquist S (1986) The heat-shock response. Ann Rev Biochem. 55:1151–1191
2. Sonna LA, Fujita J, Gaffin SL, Lilly CM (2002) Effects of heat and cold stress on mammalian gene expression. J Appl Physiol 92(4):1725–1742
3. Takayama S, Reed JC, Homma S (2003) Heat-shock proteins as regulators of apoptosis. Oncogene 22(56):9041–9047
4. Kregel KC (2002) Heat shock proteins: modifying factors in physiological stress responses and acquired thermotolerance. J Appl Physiol 92(5):2177–2186
5. Gewiese B, Beuthan J, Fobbe F, Stiller D, Mueller G, Boese-Landgraf J, Wolf, K-J, Deimling M (1994) Magnetic resonance imaging-controlled laser-induced interstitial thermotherapy. Investig Radiol 29(3):345–351
6. Roggan A, Ritz J-P, Knappe V, Germer C- T, Isbert C, Schaedel D, Mueller G (2001) Radiation planning for thermal laser treatment. Med Laser Appl 16(2):65–72
7. Nikfarjam M, Christophi C (2003) Interstitial laser thermotherapy for liver tumours. Brit J Surg 90(9):1033–1047
8. Van Der Zee J (2002) Heating the patient: a promising approach? Ann Oncol 13(8):1173–1184
9. Debes A, Willers R, Goebel U, Wessalowski R (2004) Role of treatment in childhood cancers: Distinct resistance profiles of solid tumor cell lines towards combined thermochemotherapy. Pediatr Blood Cancer 45(5):663–669

10. Hehr T, Wust P, Bamberg M, Budach W (2003) Current potential role of thermoradiotherapy for solid tumors. Onkologie 26(3):295–302
11. Colombo R, Salonia A, Da Pozzo LF, Naspro R, Freschi M, Paroni R, Pavone Malasco M, Rigatti P (2003) Combination of intravesical chemotherapy and hyperthermia for the treatment of superficial bladder cancer: preliminary clinical experience. Crit Rev Oncol/Hematol 47(2):127–139
12. Jordan A, Scholz R, Maier-Hauff K, Johannsen M, Wust P, Nadobny J, Schirra H, Schmidt H, Deger S, Loening S, Lanksch W, Felix R (2001) Presentation of a new magnetic field therapy system fort he treatment of human solid tumors with magnetic fluid hyperthermia. J Magnetism Magn Mat 235:118–126
13. Johannsen M, Thiesen B, Gneveckow U, Taymoorian K, Waldoefner N, Scholz R, Deger S, Jung K, Loening S, Jordan A (2005) Thermotherapy using magnetic nanoparticles combined with external radiation in an orthotopic rat model of prostate cancer. Prostate 66(1):97–104
14. Gellermann J, Wlodarczyk W, Hildebrandt B, Ganter H, Nicolau A, Rau B, Tilly W, Faehling H, Nadobny J, Felix R, Wust P (2005) Noninvasive magnetic resonance thermotherapy of recurrent rectal carcinoma in a 1.5 Tesla hybrid system. Cancer Res 65(13):5872–5880
15. Mack M, Straub R, Eichler K, Söllner O, Lehnert T, Vogl T (2004) Breast cancer metastasis in liver: laser-induced interstitial thermotherapy-local tumor control rate and survival data. Radiol 233(2):400–409
16. Dewhirst MW, Viglianti BL, Lora-Michiels M, Hanson M, Hoopes PJ (2003) Basic principles of thermal dosimetry and thermal thresholds for tissue damage from hyperthermia. Int J Hyperthermia 19(3):267–294
17. Park HG, Han SI, Oh SY, Kang HS (2005) Cellular responses to mild heat stress. Cell Mol Life Sci 62(1):10–23
18. Funk KRHW, Nagel F, Wanka F, Krinke, HE, Gölfert F, Hofer A (1999) Effects of heat shock on the functional morphology of cell organelles observed by video-enhanced microscopy. Anat Rec 255(4):458–464
19. Huckriede A, Heikema A, Sjollema K, Briones P, Agsteribbe E (1995) Morphology of the mitochondria in heat shock protein 60 deficient fibroblasts from mitochondrial myopathy patients. Effects of stress conditions. Virchows Arch 427(2):159–165
20. Lai YK, Lee WC, Hu CH, Hammond GL (1996) The mitochondria are recognition organelles of cell stress. J Surg Res 62(1):90–94
21. Macouillard-Poulletier de Gannes F, Leducq N, Diolez P, Belloc F, Merle M, Canioni P, Voison P-J (2000) Mitochondrial impairment
and recovery after heat shock treatment in a human microglial cell line. Neurochem Intl 36(3):233–241
22. Macouillard-Poulletier de Gannes F, Merle M, Canioni P, Voison P-J (1998) Metabolic and cellular characterization of immortalized microglial cells under heat stress. Neurochem Intl 33(1):61–73
23. Waggoner AS (1979) Dye indicators of membrane potential. Annu Rev Biophys Bioenerg 8:47–68
24. Cossarizza A, Baccarani-Contri M, Kalashnikova G, Francheschi C (1993) A new method for the cytofluorimetric analysismof mitochondrial membrane potentialusing the J-aggregate forming lipophilic cation 5,5′,6,6′-tetrachloro-1,1′,3,3′-tetraethyl- benzimidazolcarbocyanine iodide (JC-1). Biochem Biophys Res Commun 197(1):40–45
25. http://probes.invitrogen.com/servlets/spectra?fileid = 3168p82
26. http://probes.invitrogen.com/media/publications/159.pdf
27. Keshavan P, Schwemberger SJ, Smith DLH, Babcock FG, Zucker SD (2004) Unconjugated bilirubin induces apoptosis in colon cancer cells by triggering mitochondrial depolarization. Int J Cancer 112(2):433–445
28. Zunino SJ, Storms DH (2005) Resveratrol-induced apoptosis is enhanced in acute lymphoblastic leukemia cells by modulation of the mitochondrial permeability transition pore. Cancer Lett XX:1–12
29. Lieven CJ, Vrabec JP, Levin LA (2003) The effects of oxidative stress on mitochondrial transmembrane potential in retinal ganglion cells. Antioxidants & Redox Signaling 5(5):641–646
30. Wang J-L, Ke D-S, Lin M-T (2005) Heat shock pretreatment may protect against heatstroke-induced circulatory shock and cerebral ischemia by reducing oxidative stress and energy depletion. Shock 23(2):161–167
31. Dressler C, Minet O, Novkov V, Mueller G, Beuthan J (2005) Microscopical heat stress investigations under application of quantum dots. J Biomed Optics 10:1–9
32. Beuthan J, Dressler C, Minet O (2004) Laser induced fluorescence detection of quantum dots redistributed in thermally stressed tumor cells. Laser Phys 14(2):213–19
33. Crompton M (1999) The mitochondrial permeability transition pore and its role in cell death. Biochem J 341(Pt 2):233–249
34. Kim J-S, He L, Lemasters JL (2003) Mitochondrial permeability transition: a common pathway to necrosis and apoptosis. Biochem Biophys Res Commun 304(3):463–470
35. Bernardi P, Scorrano L, Colonna R, Petronelli V, Di Lisa F (1999) Mitochondria and cell death. Eur J Biochem 264:687–701
36. O'Reilly CM, Fogarty KE, Drummond RM, Tuft RA, Walsh JV, Jr (2003) Quantitative analysis of spontaneous mitochondrial depolarizations. Biophys J 85:3350–3357